Temperature dependent relaxation dynamics of luminescent NaX:Tm^{2+} (X=Cl, Br, I)

Plokker, M. P.; van der Kolk, E.

DOI
10.1016/j.jlumin.2019.116694

Publication date
2019

Document Version
Accepted author manuscript

Published in
Journal of Luminescence

Temperature Dependent Relaxation Dynamics of Luminescent NaX:Tm^{2+} (X=Cl, Br, I)

M.P. Plokker and E. van der Kolk

Luminescence Materials Research Group, Delft University of Technology, Mekelweg 15, 2629 JB Delft, The Netherlands

---

Abstract

In recent years, Thulium in its 2+ oxidation state has been identified as candidate dopant in halide hosts for luminescent solar concentrators. Yet, some of its luminescent properties with regard to these applications remain unexplored. In this study we report on the temperature dependent photo-luminescent behaviour of NaCl:Tm^{2+}, NaBr:Tm^{2+}, and NaI:Tm^{2+}. These monohalide materials demonstrate up to five distinct emission peaks which can be attributed to the $4f^{12}\rightarrow4f^{12}$ and $4f^{11}5d^{1}\rightarrow4f^{12}$ transitions of Tm^{2+}. Their time- and temperature dependent luminescence intensity behaviours are explained by a qualitative model describing the thermally stimulated radiative- and non-radiative relaxation dynamics. The behaviour of Tm^{2+} in these monohalides proves to be similar to earlier reported findings on Tm^{2+}-doped trihalide perovskites of the form $CsCaX_3$ (X=Cl, Br, I), however, the 4f-4f emission remains by far the most dominant emission between 10-300K.

1. Introduction

The luminescent properties of Tm^{2+}-doped trihalide perovskites have been charted quite intensively over the past years. Most notably by Grimm et al. [1-6], and more recently by the theoretical work of De Jong et al. [7] and experimental study by Karbowiak et al. [8]. This all mainly involved the $CsCaX_3$:Tm^{2+} (X=Cl, Br, I) series where the upconversion characteristics, quenching mechanisms and temperature dependent relaxation dynamics were investigated. Beside the earlier reported [9] 4f→4f emission of Tm^{2+}, surprisingly enough, also emissions from higher lying 5d-states were observed; albeit at low temperature. Furthermore, it was brought to light that the anion variation along the series leads to a remarkable change in the radiative and non-radiative relaxation properties and their related temperature regimes of supremacy. For non-perovskite Tm^{2+}-doped halides these attributes have been investigated to much less extent. Besides a few low temperature studies [9-12] , only a single study exists on the temperature dependent relaxation dynamics of some Tm^{2+}-doped dihalides. [13] It indisputably reveals that the temperature dependent luminescence behaviour of Tm^{2+} varies drastically over the different halide hosts. For Tm^{2+}-doped monohalides no such study exists at all. Nevertheless, their room temperature luminescent properties have recently been investigated by O.M. ten Kate et al. with the aim of exploring their potential for Luminescent Solar Concentrators (LSCs). [14] It was found that Tm^{2+}-doped halides are able to absorb up to 65% of the air mass 1.5 solar spectrum. In addition, the large Stokes' shift between the 4f→4f emission and the 5d-absorption bands of the materials entails virtually no self-absorption losses. Besides, the light emerging from the 4f→4f emission falls within the spectral absorption range of Copper Indium Selenium (CIS) solar cells and can hence be used for photovoltaic energy conversion.

All in all, the prospect of Tm^{2+}-doped halides as LSC material and the absence of a detailed analysis into the temperature dependent luminescence behaviour of the Tm^{2+}-doped alkali-monohalides, has incited us to investigate the relaxation dynamics of these latter materials. At first the different luminescent emissions of the materials are classified in accordance to their energy level-transitions as based on the luminescence excitation spectra. Subsequently, the luminescence relaxation dynamics are investigated over a broad temperature range, using temperature and time resolved measurements. The findings are used to constitute a qualitative model that is able to describe the relaxation dynamics of the materials

in a correct fashion only when non-radiative processes via conduction band states are included.

2. Experimental Section

2.1 Powder Synthesis and Preparation

The NaCl:Tm^{2+}, NaBr:Tm^{2+} and NaI:Tm^{2+} powder samples were prepared by respectively mixing NaCl, NaBr and NaI (Alfa Aeser, 99.99%) with 1% molar TmI_2 powder (Sigma Aldrich, 99.9%) under inert conditions. The mixtures were stored in quartz ampoules. The ampoules were then individually sealed off by a vacuum valve and connected to a KF-vacuum system that evacuated them towards a pressure of 10^{-2}mbar. Subsequently, a conventional Tecla burner was used to heat the ampoules until the powder liquefied. The burner was switched off typically after 3 minutes as the mixture started to boil momentarily. After that, the ampoules were cooled back to room temperature and the resulting samples were crushed to powder in a glovebox. For all powder characterisation measurements, specially designed sample holders, similar to those described by Rogers et al. [15], were employed to protect the samples against hygroscopicity and oxidation reactions.

2.2 Powder Characterisation

ICP-OES measurements were used to check the Tm concentrations in the samples; which were respectively found to be: 0.69%, 0.75% and 1.0% for NaCl:Tm^{2+}, NaBr:Tm^{2+} and NaI:Tm^{2+}. In addition, the crystal structure of the powder samples was monitored using X-ray diffraction and all were found to exhibit the NaCl structure type ($Fm\bar{3}m$), as elucidated in the supplementary information. For NaCl:Tm^{2+} the presence of a very weak NaI phase was observed, which is most likely related to Iodine originating from the TmI_2 starting powder. The corresponding NaCl:NaI peak intensity ratio was estimated to be 100:3 at most. Furthermore, diffuse reflectance measurements, presented in the supplementary information, revealed the presence of small quantities of Tm^{3+}. Yet, the selected wavelength of excitation of 420nm does not overlap with any of the Tm^{3+} excitation bands, as explicated in the Dieke diagram. [16] In addition, no energy transfer between Tm^{2+} and Tm^{3+} was observed.

Finally, fluorescence quantum yield measurements were performed using an Edinburgh FLS980 integrating sphere with a 450W Xenon arc lamp and Hamamatsu C9940-02 NIR-PMT. Upon excitation into their lowest energy 5d-bands, internal quantum efficiencies of 16±1%, 32±2%, and 33±2% were respectively found for NaCl:Tm^{2+}, NaBr:Tm^{2+} and NaI:Tm^{2+}.

2.3 Luminescence Properties

For excitation of the powder samples, either a Xenon lamp coupled to a double monochromator with three gratings or a tuneable EKSPLA laser was used. In addition, the samples were cooled or heated using a APD Cryogenic Helium cooler with Lakeshore temperature controller. Furthermore, the luminescence emerging from the samples was measured using a Hamamatsu C9100-13 EM-CCD or H1033A-75 NIR-PMT that are respectively sensitive between 400-1150nm and 950-1600nm and that are attached to a single monochromator with three gratings. The wavelength dependent detection efficiency of the detectors was established using a calibrated EPLAB NBS 1000W Quartz Iodine lamp. In addition, the overlap in detection of the 1140nm 4f→4f emission peak of Tm^{2+} allowed us to scale the relative output of both detectors. Time resolved measurements were performed by connecting a DT5724F (0-2ms) or DT5730 (0-40ms) CAEN digitiser to the same NIR-PMT or a Hamamatsu R7600U-20HV-800V PMT. The related decay curves were acquired by averaging 1000 individual laser excited spectra.

3. Results and Discussion

3.1 Classification of Emissions

The well-known NaCl ($Fm\bar{3}m$) crystal structure type of the three samples implies that the Tm^{2+} ions that occupy the Na^{+}-lattice sites are octahedrally coordinated, leading to a 5d-crystal field splitting where the t_{2g} levels are situated below those of the e_g levels. However, it should be noted that the incorporation of the Tm^{2+}-dopants must result in the formation of charge compensating defects, that will distort the perfect octahedron and by consequence the related crystal field splitting. Charge compensating mechanisms in monohalides have been described extensively by Rubio et al. [17] for ions such as Eu^{2+}. Nevertheless,

a description of the 5d-states assuming an octahedral symmetry still remains a useful first order approximation that will be adopted here.

Figure 1 shows the excitation spectra of the three different powders at 20K. The overall shape of the spectra is quite similar, particularly at low energy. Besides, the shapes are quite identical to the room temperature absorption spectra found previously by ten Kate et al. for the NaX:3%Tm^{2+} (X=Cl, Br, I) series. [14]

The 5d-levels of Tm^{2+} are split several times and most prominently by: the crystal field interaction, the Coulomb repulsion and spin orbit coupling within the $4f^{12}$-configuration, the Coulomb repulsion between the 4f and 5d electrons, and the spin-orbit interaction of the 5d-electron. The first interaction causes for a splitting in a doublet e_g and a triplet t_{2g}, whereas the second interaction results in an additional splitting into $^{2S+1}L_J$ terms which are analogous to the Tm^{3+} multiplets in the Dieke diagram. In addition to that, the third interaction results in a further splitting into spin S=1/2 and S=3/2 states and the fourth interaction splits the levels even further. A more detailed discussion about the structure of the $4f^{12}5d^1$ configuration of Tm^{2+} can be found in the work of Grimm et al. [2] and De Jong et al.. [7]

Based on our acquired spectra, two main sets of excitation bands can be distinguished; as indicated by the dashed lines in figure 1. For NaBr:Tm^{2+} the bands of the first set are located at around 433nm and 497nm; and those of the second set are positioned close to 568nm and 656nm. A brief calculation reveals that the difference between the highest energy band of each set amounts to 5490cm^{-1}. Similarly, the mutual difference between the lowest energy bands amounts to 4880cm^{-1}. This corresponds fairly well to the difference of 5700cm^{-1} between the $^3F_4$ and $^3H_6$ levels of Tm^{3+} in the Dieke diagram.

The set of excitation bands located at longer wavelength can thus be related to the $(^3H_6,t_{2g})$ levels of Tm^{2+}; while the two excitation bands located at shorter wavelength correspond to the $(^3F_4,t_{2g})$ levels.

A quick verification of all this is offered via work of Rubio et al. on NaCl:Eu^{2+} [17], where the lowest energy 4f-5d absorption band is observed at around 400nm. Subtracting the material independent energy difference of 1.27eV, as explicated by Dorenbos et al. [18], the lowest energy 5d-band for NaCl:Tm^{2+} should be located at 676nm. This falls almost exactly on the assigned position of the $(^3H_6,t_{2g})$ band. In addition, a weak excitation band is observed for NaI:Tm^{2+} at around 850nm. It can be classified as the $(^3H_6,t_{2g})_{S=3/2}$ band and in contrast to the previous spin-allowed bands it is spin-forbidden. [2]

Upon varying the anion species from Cl to Br to I, it can be observed that the designated excitation bands gradually shift towards longer wavelengths. This can be related to nephelauxetic effects and a change in crystal field strength as caused by slight changes in the Tm-anion distances.

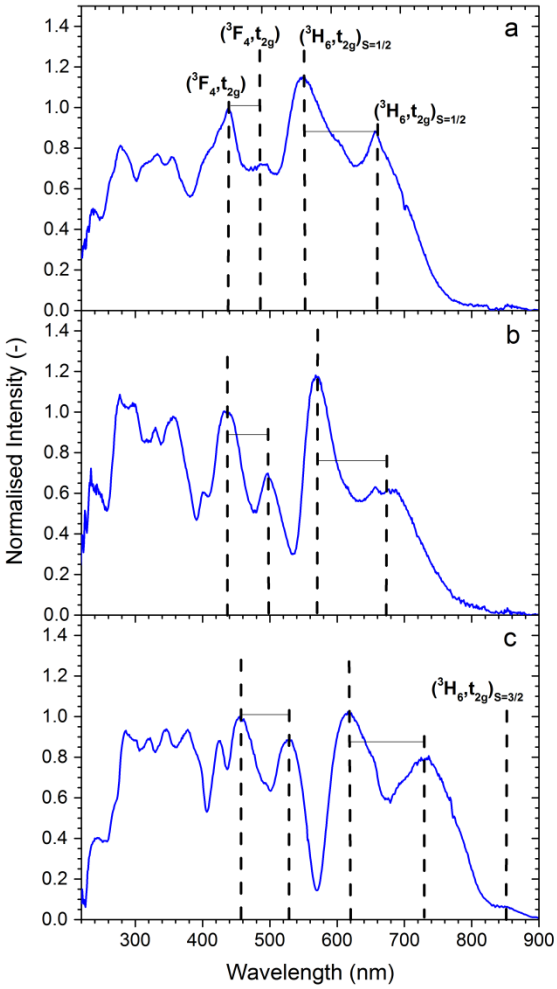

Figure 1: The excitation spectra of: a NaCl:Tm^{2+}, b NaBr:Tm^{2+}, and c NaI:Tm^{2+} as acquired monitoring the 4f-4f emission peak of Tm^{2+} at 20K at 1140nm. The main excitation bands are designated and normalised on the $(^3F_4,t_{2g})$ band.

The emission spectra in figure 2 reveal up to five distinct Tm^{2+} emissions that are present at 20K for all three materials. The emissions are labelled A to E in analogy to the work of Grimm et al. [6] Their wavelengths and decay times are provided in table 1. Furthermore, a schematic representation of the different 5d→4f and 4f→4f emissions is displayed for convenience in figure 3.

The previously assigned excitation bands together with Stokes' shift values, provide a means to classify the emissions in accordance to their transitions. The Stokes' shift energy values for NaCl, NaBr, and NaI as based on the Eu^{2+} 5d→4f emission respectively amount to 0.12eV, 0.13eV, and 0.19eV. [17] Upon addition of these values with the Tm^{2+} 5d→4f emissions, a good resemblance is obtained with the bands observed in the excitation spectra presented in figure 1. Emission D in NaBr:Tm^{2+} is perceived at 511nm as can be seen in figure 2b. If we subtract the Stokes' shift energy for NaBr of 0.13eV we should have an excitation band at 486nm. Figure 1b indeed shows an excitation band, which is very close to 500nm. Therefore, we assign emission D to a transition from the $(^3F_4,t_{2g})$ levels to the $^2F_{7/2}$ groundstate. It has been observed before in Tm^{2+}-doped di- and trihalides. [2,4,6,8] In addition, its relatively short decay time of 1015ns at 20K reflects the parity-allowed nature of a typical 5d→4f transition.

In a similar manner, the wavelength of emission C can be coupled to an excitation band located at 676nm, which represents the spin-allowed $(^3H_6,t_{2g})_{S=1/2}$-band. Hence, emission C can be associated with $(^3H_6,t_{2g})_{S=1/2}\rightarrow{}^2F_{7/2}$ transition. Furthermore, emission B located at 804nm should correspond to an excitation band at 740nm. For NaBr:Tm^{2+} this band is not clearly observed, but it most likely represents the spin-forbidden $(^3H_6,t_{2g})_{S=3/2}$-band; which is only observed for NaI:Tm^{2+} at around 850nm. Therefore the transition related to emission B is indicated by the spin-forbidden $(^3H_6,t_{2g})_{S=3/2}\rightarrow{}^2F_{7/2}$ transition. The dissimilarity in decay time between emissions C and B of 5 to 59µs and 432µs respectively reflects their spin-allowed and spin-forbidden nature.

Besides, for the NaCl:Tm^{2+} sample, two distinct B emissions are observed. This is most likely associated with the presence of two different luminescence centres as a result of the charge compensating mechanisms. Moreover, emission C was not observed for this material. Its absence is also echoed by previous studies performed on Tm^{2+}-doped halides that involve chloride as anion species. [4,5,13]

The energy of emission E corresponds well to the energy gap between the $^3F_4$ and $^2F_{5/2}$ levels. In addition, the energy difference of emission D and E is exactly equal to the energy difference between the $^2F_{5/2}$ and $^2F_{7/2}$ 4f levels. Emission E can therefore be attributed to the $(^3F_4,t_{2g})\rightarrow{}^2F_{5/2}$ transition and has previously been reported only for Tm^{2+}-doped halide perovskites. [1,4-6,13] Moreover, emission E is clearly observed in case of NaBr:Tm^{2+}, while for NaCl:Tm^{2+} it is present as a weak shoulder of emission B.

Lastly, the wavelength of emission A perfectly matches the wavelength difference between the $^2F_{5/2}$ and $^2F_{7/2}$ 4f levels. It can be related to the $^2F_{5/2}\rightarrow{}^2F_{7/2}$ transition as observed many times before. [1,4-6,8,9,13] In addition, it has a relatively long decay time of 4.2ms at 20K, which is archetypal for non-parity allowed 4f-4f transitions.

As an overall observation, all 5d-4f emissions gradually shift towards longer wavelength upon varying the anion from Cl to Br, and finally I. For NaBr:Tm^{2+} the average shift with respect to NaCl:Tm^{2+} is around 16nm, while for NaI:Tm^{2+} it is close to 58nm.

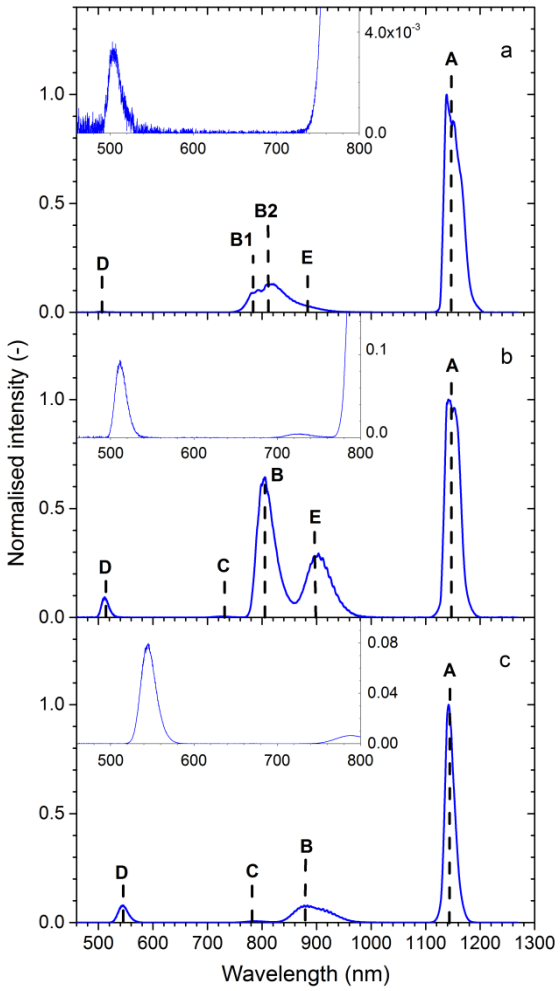

Figure 2: The emission spectra of: a) NaCl:Tm^{2+}, b) NaBr:Tm^{2+}, and c) NaI:Tm^{2+} as photo-excited at 420nm and recorded at 20K. The emissions are corrected for the detector sensitivities to allow for a relative comparison in intensity. Furthermore, their peak intensities are normalised on that of emission A.

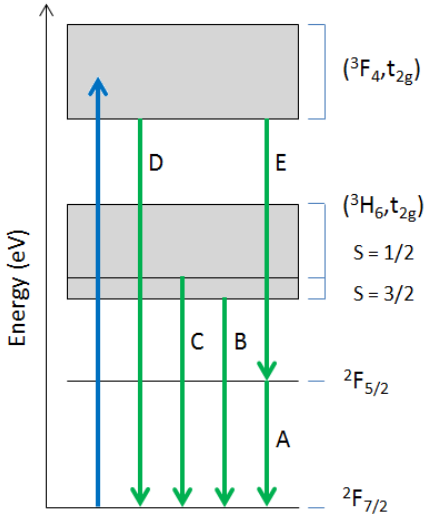

Figure 3: Schematic overview of the five observed Tm^{2+} emissions, taking into account the Stokes´ shifts. The photoexcitation wavelength of 420nm falls within the $(^3F_4,t_{2g})$ band.

3.2 Temperature and time dependent emissions

With the emissions now classified in accordance to their transitions, the temperature dependence of the luminescence intensity and decay time were investigated between 10 and 300K. In the following, each emission A through E will be presented and discussed sequentially. The acquired intensity and time resolved results are summarised in Arrhenius plots that are respectively presented in figures 4 and 5.

Table 1: Classification and properties of the observed Tm^{2+} emissions in NaCl:Tm^{2+}, NaBr:Tm^{2+}, and NaI:Tm^{2+}.

Sample [-]	Emission [-]	Transition [-]	Wavelength [nm] (20K)	Energy [eV] (20K)	Decay Time (20K)	Relative Integrated Intensity [-] (20K)
NaCl:Tm^{2+}	D	$(^3F_4,t_{2g}) \rightarrow {}^2F_{7/2}$	503	2.47	120ns	1
	B1	$(^3H_6,t_{2g})_{S=3/2} \rightarrow {}^2F_{7/2}$	779	1.60	380µs	24
	B2	$(^3H_6,t_{2g})_{S=3/2} \rightarrow {}^2F_{7/2}$	811	1.53	400µs	4
	E	$(^3F_4,t_{2g}) \rightarrow {}^2F_{5/2}$	883	1.41	-	2
	A	${}^2F_{5/2} \rightarrow {}^2F_{7/2}$	1139	1.09	2.7ms	52
NaBr:Tm^{2+}	D	$(^3F_4,t_{2g}) \rightarrow {}^2F_{7/2}$	511	2.43	1.0µs	7
	C	$(^3H_6,t_{2g})_{S=1/2} \rightarrow {}^2F_{7/2}$	728	1.71	5.0 µs, 59µs	1
	B	$(^3H_6,t_{2g})_{S=3/2} \rightarrow {}^2F_{7/2}$	804	1.55	430µs	28
	E	$(^3F_4,t_{2g}) \rightarrow {}^2F_{5/2}$	898	1.38	710ns	9
	A	${}^2F_{5/2} \rightarrow {}^2F_{7/2}$	1142	1.09	4.2ms	33
NaI:Tm^{2+}	D	$(^3F_4,t_{2g}) \rightarrow {}^2F_{7/2}$	545	2.28	810ns	6
	C	$(^3H_6,t_{2g})_{S=1/2} \rightarrow {}^2F_{7/2}$	789	1.58	12µs, 51µs	1
	B	$(^3H_6,t_{2g})_{S=3/2} \rightarrow {}^2F_{7/2}$	877	1.42	440µs	22
	A	${}^2F_{5/2} \rightarrow {}^2F_{7/2}$	1142	1.09	3.7ms	54

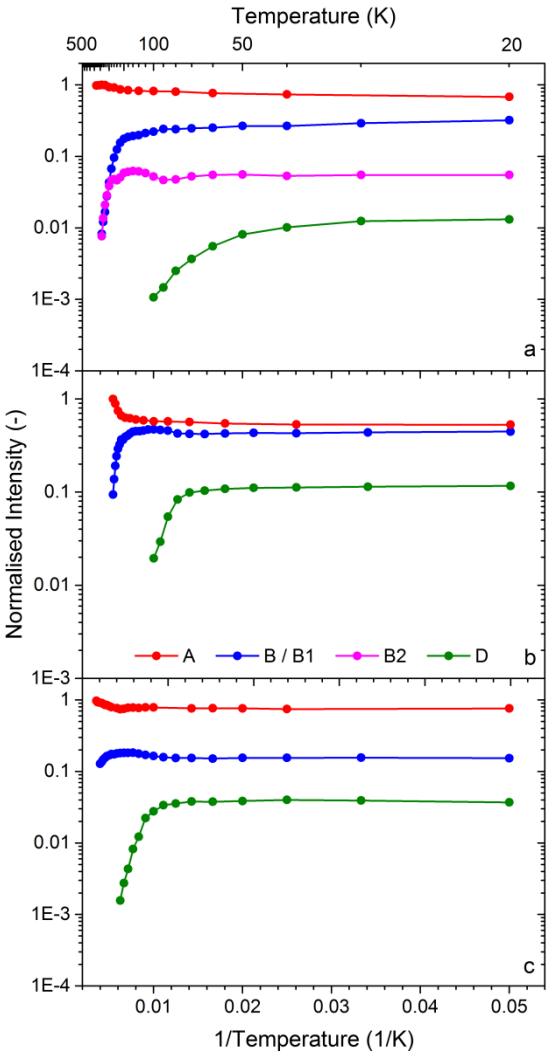

Figure 4: Arrhenius plots of the integrated emission intensity of the different types of Tm^{2+} emissions between 20 and 300 K for a) NaCl:Tm^{2+}, b) NaBr:Tm^{2+}, and c) NaI:Tm^{2+}. The curves are normalised on emission A at 300K. The data was obtained after 420nm excitation.

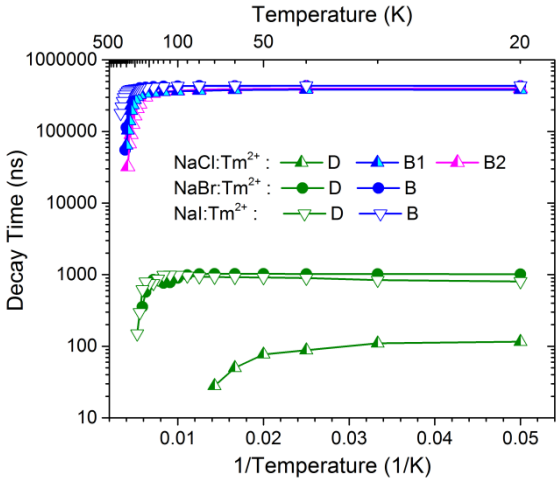

Figure 5: Arrhenius plot containing the temperature dependence of the luminescence lifetimes of emissions A and C for all three studied materials. The original decay curves were acquired using 10ns pulsed laser excitation at 420nm.

Emission D

Emission D emerges from a higher energy 5d-state, which in regard to all lanthanide ions has so far only been observed for Tm^{2+}. Its presence has been reported before in $CsCaX_3:Tm^{2+}$ (X = Cl, Br, I) and $ACl_2:Tm^{2+}$ (A = Ca, Sr) [1,3-6,13]. In this study, both its temperature and time dependence are reported for the first time, as can respectively be seen from the green curves in figures 4 and 5. In addition, temperature dependent emission spectra of emission D in NaBr:Tm^{2+} are provided in figure 6a, from which it can be observed that the luminescence intensity starts to decrease rapidly at a temperature close to 80K and has quenched completely at 170K. This is also perceived from the Arrhenius plot in figure 4b, from which a thermal deactivation energy of 54meV could be retrieved. For NaCl:Tm^{2+} and NaI:Tm^{2+}, the related emission spectra presented in the supplementary information reveal a very similar temperature behaviour. Specifically, for NaCl:Tm^{2+} emission D already starts to quench at a temperature of 20K. At 100K it is no longer observed. The related thermal deactivation energy amounts to 30meV. For NaI:Tm^{2+}, emission D starts to quench at 90K and at 190K it has fully quenched, providing a thermal deactivation energy of 86meV. These trends in thermally stimulated quenching behaviour are confirmed by the decay spectra shown for NaBr:Tm^{2+} in figure 6b. For increasing temperature the luminescence lifetime decreases. The lifetime-temperature Arrhenius plots in figure 5 reveal that for NaBr:Tm^{2+} the luminescence lifetime has decreased from 1.0µs at a temperature of 20K to 360ns at 170K. Similarly, the lifetimes of NaCl:Tm^{2+} and NaI:Tm^{2+} respectively decrease from 120ns at 20K to 28ns at 70K, and from 810ns at 20K to 150ns at 190K. Upon a closer inspection, the energy difference between $(^3F_4,t_{2g})$ and the $(^3H_6,t_{2g})_{S=1/2}$ levels of NaX:Tm^{2+} (X=Cl, Br, I) respectively amounts to around 283meV, 320meV, and 330meV. Their ascending order reflects the respective higher temperatures of quenching: emission D quenches first for NaCl:Tm^{2+}, followed by NaBr:Tm^{2+}, and finally NaI:Tm^{2+}. In addition, the values are close to those found previously for

other Tm^{2+}-doped halides and typically represent a few phonon energies at most. [1,4,6,8,13] The related quenching mechanism can then most likely be attributed to temperature dependent multi-phonon relaxation, as was previously also concluded by Grimm et al. [1,4,6] The peculiar evolution in shape of the decay spectra in figure 6b are also seen for emission D in NaCl:Tm^{2+} and NaI:Tm^{2+} as can be witnessed in the supplementary information. Below 100K a single exponential decay is observed. Toward higher temperatures a fast component develops and finally the slower components start to quench as well. At the moment we have no clear explanation for this unusual behaviour.

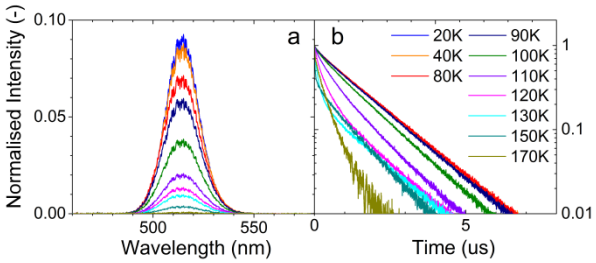

Figure 6: The temperature dependent emission spectra (a) and decay spectra (b) of emission D in NaBr:Tm^{2+} as respectively photo- or laser excited at 420nm. The emission spectra are normalised on emission A at 20K.

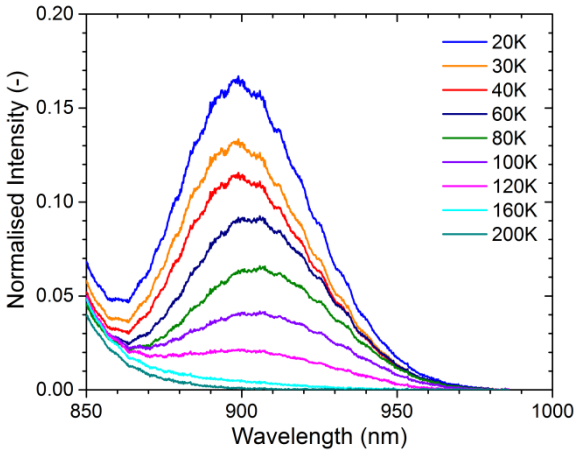

Figure 7: Temperature dependent emission spectra of emission E in NaBr:Tm^{2+} as photoexcited at 420nm. The spectra are normalised on the peak of emission A at 20K.

Emission E

As emission E originates from the same energy level as emission D, the temperature dependence of the emission intensity and decay time values should be equivalent. This is true to a large extent. Figure 7 displays the temperature dependent emission spectra of emission E in NaBr:Tm^{2+}. Much like emission D, the intensity of emission E decreases within the temperature range of 20K to 200K. The decline is about 50% from 20K to 80K, indicating that the temperature dependence of emission E lies indeed in the same range of that of emission D. Furthermore, the related decay times of emission D and E are 1.0µs and 710ns at 20K respectively, and 900ns and 450ns at 100K. Since the wavelength of emission E lies in a range where the Hamamatsu R7600U-20HV-800V PMT has a very low efficiency, we had to increase the laser power by more than a factor 10. This may have caused the decay spectra of emission E to become slightly non-exponential and develop a fast component, which makes a more detailed quantitative comparison speculative. In NaCl:Tm^{2+} emission E can also be observed, but only as a weak shoulder of emission B. The related temperature dependent emission spectra are plotted in the supplementary information. No reliable temperature dependent intensity values or decay times could be obtained. For NaI:Tm^{2+}, emission E should be expected at a wavelength of around 1040nm, but it was not observed.

Emission B

From the temperature dependent emission spectra of NaBr:Tm^{2+} in figure 8a, it can be deduced that the luminescence intensity of emission B gradually decreases over temperature. The blue curve in figure 4b provides a more detailed insight, where two downward slopes can be distinguished. This indicates that emission B undergoes quenching in two different stages. The first stage is already active at 20K and can be attributed to 5d-4f multi-phonon relaxation [1,4,13] with a weak temperature dependence, while the second stage setting in at around 170K is related to thermal stimulated quenching with a much higher thermal deactivation energy. This latter process involves relaxation via the cross point between the $^3H_{6\ S=3/2}$ and $^2F_{5/2}$ parabolas in the configuration diagram, for which a certain amount of thermal energy is required. By comparison, the thermal deactivation energy of the first process amounts to around 0.13meV, whereas that of the second process comes close to 136meV. For NaCl:Tm^{2+} and NaI:Tm^{2+} the first quenching process also commences at 20K with respective thermal

deactivation energies of 0.17meV and 0.13meV, whereas the second process respectively sets in at around 190K and 150K with deactivation energies of 189meV and 27meV.

The quenching of emission B predicts a shortening of its luminescence lifetime. Figure 8b shows that for NaBr:Tm^{2+} this is indeed true. Furthermore, the blue curve in the lifetime-temperature plots in figure 5 reveals that the decay time decreases from 430µs at 20K to 55µs at 260K. The decay spectra of NaCl:Tm^{2+} and NaI:Tm^{2+} in the supplementary materials also acknowledge this behaviour. For the former material, the decay time respectively decreases from 380µs and 400µs at 20K to 100µs and 32µs at 240K; and for the latter it changes from 440µs at 20K to 180µs at 300K. The close resemblance in the behaviour of the luminescence intensity and lifetime is expected since both are essentially caused by the same quenching process. The increased quenching of emissions D and E with temperature, as initiated by 5d-5d multi phonon relaxation, should cause for an increased feeding of the lowest 5d-state from which emission B originates. In essence, a decrease in the intensity of emissions D and E should then result in an increase in the intensity of emission B. The respective decrease and increase would be equal only if the quantum efficiency of emission B is 100%, which is not the case as 4f-4f emission A dominates. Yet, a slight increase in the intensity of emission B can be seen in figure 4b and c, exactly within the same temperature range where emission D starts to decrease.

Emission C

Previously, emission C has been observed in $CsCaX_3$:Tm^{2+} (X = Br, I). [1,4-6] The temperature dependent emission spectra in figure 9 reveal that it is only present for NaBr:Tm^{2+} and NaI:Tm^{2+} and that it is most intense at 20K. For NaBr:Tm^{2+} it already starts to undergo quenching at this temperature and has quenched completely at 140K. For NaI:Tm^{2+}, the quenching of emission C also commences at 20K. Yet, it remains present all the way up to room temperature. Since the energy difference between the $^3H_{6\ S=1/2}$ and $^3H_{6\ S=3/2}$ levels is around 260meV for NaI:Tm^{2+}, the related quenching mechanism can most likely be attributed to multi-phonon relaxation. For NaCl:Tm^{2+} the absence of this emission was earlier described for $CsCaCl_3$:Tm^{2+} [4] by a highly efficient quenching. The relatively low intensity of the emission and the overlap with emission B has prevented a further temperature analysis of its intensity and its luminescence decay.

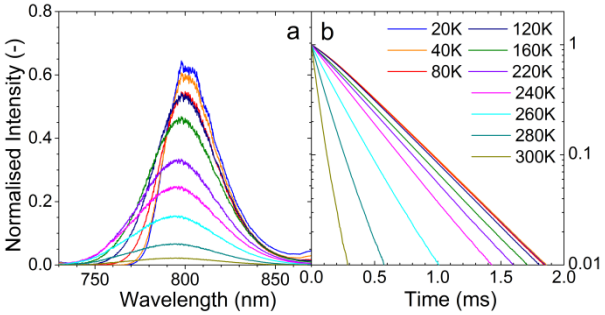

Figure 8: The temperature dependent emission spectra (a) and decay spectra (b) of emission B in NaBr:Tm^{2+} as respectively photo- or laser excited at 420nm. The emission spectra are normalised on emission A at 20K, while the decay spectra are normalised on their origin.

Emission A

As perceived in the previous section, emission A is already present at 20K for all of the three studied materials. Figure 10 shows that its intensity gradually increases over temperature. Moreover, the red curve in figure 5 with the integrated emission intensity reveals that for NaBr:Tm^{2+} this increase happens in two different stages, as witnessed by the two upward slopes in the plot. The first stage is observed up to a temperature of 200K, after which the second stage clearly starts to manifests itself. At around the very same temperature, emission B displays an anti-correlated behaviour that can also be noticed for NaCl:Tm^{2+} and NaI:Tm^{2+}, although somewhat less clear.

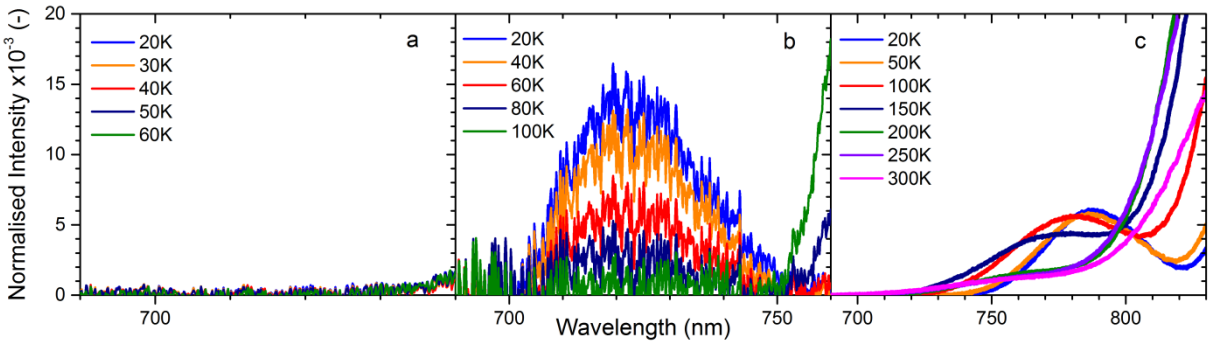

Figure 9: The temperature dependent emission spectra of emission B in: a) NaCl:Tm^{2+} (no B-emission), b) NaBr:Tm^{2+}, and c) NaI:Tm^{2+} as photo-excited at 420nm. The spectra are normalised on emission E at 20K.

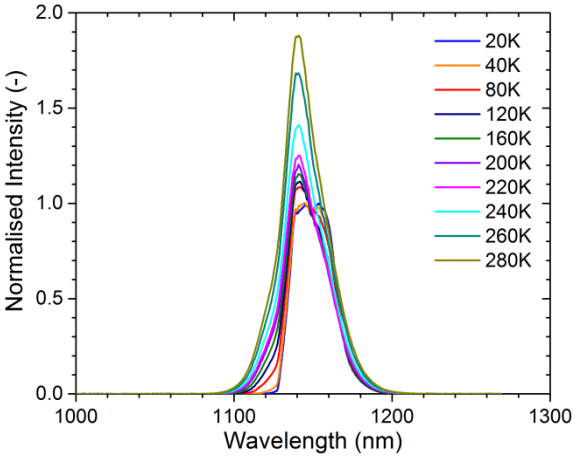

Figure 10: The temperature dependent emission spectra of emission A in NaBr:Tm^{2+} as photo-excited at 420nm. The spectra are normalised on the emission peak at 20K.

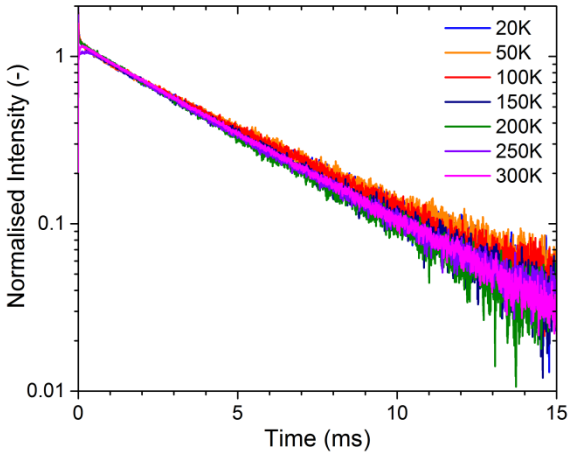

Figure 11: The decay spectra of emission A in NaBr:Tm^{2+} for different temperatures as laser excited at 420nm.

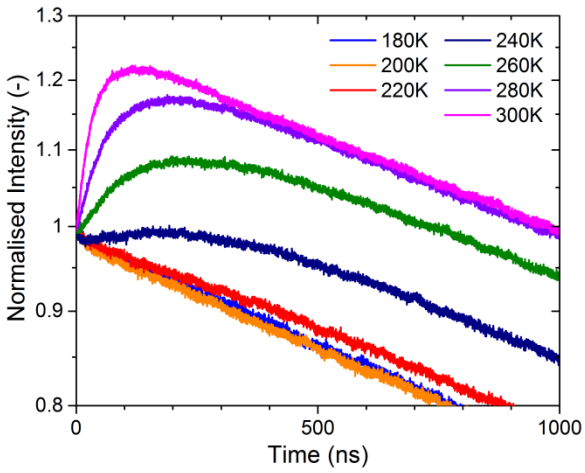

Figure 12: The decay spectra of emission A in NaBr:Tm^{2+} plotted at a short time scale between 180 and 300K. The decay curves were acquired using pulsed laser excitation at 420nm and clearly exhibit a rise time phenomena for temperatures above 200K.

The decay curves in figure 11 reveal that the luminescence lifetime of emission A remains constant with temperature. This indicates that as soon as the $^2F_{5/2}$ 4f level is populated by the higher energy 5d levels, there is no quenching of the 4f-4f emission itself. For NaCl:Tm^{2+} and NaI:Tm^{2+}, the decay curves of emission A are single exponential with respective decay times 2.7ms and 3.7ms and without any temperature dependence.

The thermally stimulated quenching of emission B and the directly related thermally stimulated feeding of emission A, predicts an initial rise in the 4f-4f decay spectrum on a timescale that corresponds to the decay time of emission B. Figure 12 shows that such a temperature dependent rise time actually exists. At temperatures below 220K, where there is no significant thermally stimulated excitation, there is no rise time. Below this temperature, the presence of 4f-4f emission A must be due to 5d-4f multi-phonon relaxation, as mentioned previously by Grimm et al.. [1,4,13]

Above 200K, the thermally stimulated excitation becomes active and a corresponding rise time evidently develops, which enhances the total 4f-4f emission intensity. The rise time becomes shorter as the temperature increases further, indicating that the feeding of the $^2F_{5/2}$ 4f level starts to happen at a faster rate. No clear rise time phenomena was witnessed for NaCl:Tm^{2+} and NaI:Tm^{2+}, possibly due to the smaller amplitude related to the intensity increase of emission A.

4. Overall Discussion

Our findings can be summarised with a qualitative model that we exemplify for NaBr:Tm^{2+} below with the aid of figures 13a and 13b. The simplest situation is encountered at room temperature. All non-radiative 5d-5d and 5d-4f relaxation processes dominate the radiative transitions so that excitation in the high energy 5d states results almost exclusively in emission A as indicated by the red arrows in figure 13b. At the lowest measured temperature of 20K the situation is far more complex. Excitation in the high energy 5d states results in emissions: A, B, C, D, and E with a relative intensity of 33, 28, 1, 7, and 9.

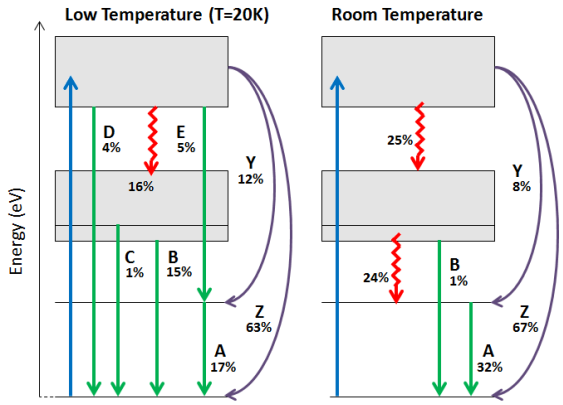

Figure 13: Schematic overview of the two proposed non-radiative channels Y and Z together with the observed emissions and quenching processes as present at low temperatures of 20K and room temperature. Percentage labels are provided to account for the dominance of the different pathways.

When it is assumed that there are no non-radiative 5d-5d relaxation processes active, the intensity of emission E should be equal to that of emission A and in addition emissions C and B should be absent. This is clearly not what is observed in figure 2. If we allow for non-radiative 5d-5d multi-phonon relaxation as indicated by the red curly arrows in figure 13, the presence of emission C and B can be explained but emissions E and A should still have the same intensity which is not the case.

Grimm et al. also opted for a very efficient non-radiative process from the higher energy 5d state to the emitting 4f level. [4] If such a non-radiative channel is assumed, as indicated by Y, emission E can be of lower intensity than emission A which is what we observe.

The non-radiative channel Y might be a photo-excited electron delocalisation to conduction band states followed by a strong relaxation to the emitting 4f level. Such a strong relaxation process has been observed before in for example [19-21]. It is plausible to assume that this relaxation process not only excite the emitting 4f level but also results in a direct return to the groundstate level, as indicated by channel Z in figure 13a. This would cause a lower than unity quantum efficiency for emission A. If a Vacuum Referred Binding Energy diagram (VRBE) is constructed for the mono-halides [22] it becomes clear that the higher energy 5d states are located in the conduction band which is a requirement for the non-radiative channels Y and Z.

With help of an integrating sphere, the internal quantum efficiency of the Tm^{2+} 4f-4f emission at room temperature was measured to be 32% at room temperature and estimated on 17% at 20K using figure 4b and table 1. So in summary, upon excitation into the higher energy 5d state of Tm^{2+}, 63% of the excitations return non-radiatively towards the groundstate via channel Z and 12% relaxes to the emitting 4f level through channel Y. In addition, 16% of the excitations relax to the lowest energy 5d state via multi-phonon relaxation, resulting in an identical 15% of emissions B plus C. Furthermore, 5% of the excitations result in emission E, followed by an equal amount of emission A. In combination with the earlier mentioned 12% this adds up to 17%, which is the QE at 20K that we estimated. Finally 4% of excitations result in emission D.

The processes related to channel Y and Z are known to be only weekly dependent on temperature [20] and should therefore have similar efficiency at room temperature. So now we may assume that at room temperature, after excitation into the higher energy 5d state of Tm^{2+}, 67% of the excitations return to the groundstate non-radiatively by channel Z and 8% to the emitting 4f level through channel Y. In addition, 25% of the excitations will relax to the lowest energy 5d state, followed by either 1% in emission B or a thermally stimulated relaxation to the emitting 4f level causing 24% of emission A. Together with the 8% that feeds this level through channel Y, this adds up to 32% which is the QE recorded at room temperature.

Although our temperature resolved intensity and decay data display clear trends for the NaX:Tm^{2+} (X=Cl, Br, I) series, which can qualitatively be well explained in a consistent manner, a more quantitative modelling involving all data using for instance rate equations proved unsuccessful. Our experimental data and the work of Rubio et al. [17] has given us some ideas why this might be the circumstance. First of all, as discussed in section 3.1, we can expect that for all materials there might be multiple Tm^{2+}-sites present because of the necessity for charge compensation when Tm^{2+} enters the mono-halides on the Na^{+}-site. Even though there is a dominant site with an octahedral coordination, there are many distorted sites

reported in literature for Eu^{2+}-doped mono-halides [17], that can all have slightly different relaxation dynamics properties. Secondly our samples are all hygroscopic and sensitive to oxidation. Despite the fact that these were stored in a glovebox and loaded in specially sealed sample holders, the samples may still have deteriorated over time due to imperfect sealing and the several months over which all measurements were performed. Finally, we have seen that in Eu^{2+}-doped NaCl and NaI, photochromic behaviour involving the photo-creations of colour centres can occur. It may therefore be that our Tm^{2+}-doped samples suffer from the same behaviour, which goes on the expense of reproducibility. We therefore believe that a more detailed and quantitative discussion of our results would become too speculative.

5. Conclusion

Luminescence behaviour of NaCl:Tm^{2+} and NaBr:Tm^{2+} are similar to Tm^{2+} doped perovskites as five different types of emissions are observed. For NaI:Tm^{2+} four emissions are observed and the behaviour is therefore similar to most of the previously investigated Tm^{2+}-doped dihalides: $CaCl_2$:Tm^{2+} and $SrCl_2$:Tm^{2+}. However, in contrast to these materials, the 4f-4f emission in the three studied monohalides is by far the most dominant emission at all temperatures; much like $RbCaI_3$:Tm^{2+} and $BaCl_2$:Tm^{2+}. This is tentatively explained by a non-radiative pathway involving conduction band states. In view of the LSC application, the supremacy of the 4f-4f emission is highly beneficial; yielding potentially large power outputs. On the other hand, the foremost non-radiative pathway forms a restriction on the QE of the materials. For further research it is recommended to perform a similar study on Tm^{2+}-doped dihalides and trihalides to investigate if the observed radiative and non-radiative processes and related QE values follow the same temperature dependence.

6. Acknowledgement

This research is financially supported by the Nederlandse Organisatie voor Wetenschappelijk onderzoek (NWO) as part of the LumiCon proposal. The authors would like to thank P. Dorenbos for helpful discussion on the excitation spectra and E. Merkx for help with the deconvolution of emission B in NaCl:Tm^{2+}. Special thanks go out to R.D. Abellon (TU Delft) and B.E. Terpstra (TU Delft) for experimental support with respectively the QE and ICP-OES measurements.

7. References

[1] E. Beurer, J. Grimm, P. Gerner, H.U. Güdel, Absorption, Light Emission, and Upconversion Properties of Tm^{2+}-doped $CsCaI_3$ and $RbCaI_3$, Inorg. Chem. 9901-9906 (2006) 45.

[2] J. Grimm, E. Beurer, H.U. Güdel, Crystal Absorption Spectra in the region of 4f-4f and 4f-5d Excitations in Tm^{2+}-doped $CsCaCl_3$, $CsCaBr_3$, and $CsCaI_3$, Inorg. Chem. 10905-10908 (2006) 45.

[3] E. Beurer, J. Grimm, P. Gerner, H.U. Güdel, New Type of Near-Infrared to Visible Photon Upconversion in Tm^{2+}-doped $CsCaI_3$, J. AM. CHEM. SOC. 3110-3111 (2006) 128.

[4] J. Grimm, J.F. Suyver, G. Carver, H. U. Güdel, Light-Emission and Excited-State Dynamics in Tm^{2+} Doped $CsCaI_3$, $CsCaBr_3$, and $CsCaI_3$, J. Phys. Chem. B 2093-2101 (2006) 110.

[5] J. Grimm, E. Beurer, P. Gerner, H.U. Güdel, Upconversion Between 4f-5d Excited States in Tm^{2+}-Doped $CsCaCl_3$, $CsCaBr_3$, and $CsCaI_3$, Chem. Eur. J. 1152–1157 (2007) 13.

[6] J. Grimm, H.U. Güdel, Five different types of spontaneous emission simultaneously observed in Tm^{2+} doped $CsCaBr_3$, Chemical Physics Letters 40–43 (2005) 404

[7] M. de Jong, D. Biner, K.W. Krämer, Z. Barandiarán, L. Seijo, A. Meijerink, New Insights in $4f^{12}5d^1$ Excited States of Tm^{2+} through Excited State Excitation Spectroscopy, J. Phys. Chem. Lett. 2730-2734 (2016) 7.

[8] M. Karbowiak, R. Lisiecki, P. Solarz, J. Komar, and W. Ryba-Romanowski, Spectroscopic peculiarities of $CsCaI_3$:Tm^{2+} single crystals examined through one-photon and excited state excitation spectroscopy, J. Alloy. Comp. 1165-1171 (2018) 740.

[9] Z.J. Kiss, Energy levels of divalent Thulium in CaF_2, Phys. Rev. 718-724 (1962) 127.

[10] H.A. Weakliem, C.H. Anderson, and E.S. Sabisky, Magnetic Circular Dichroism Spectra of Divalent Lanthanide Ions in Calcium Fluoride, Phys. Rev. B 4354-4365 (1970) 11.

[11] R.C. Alig, R.C. Ducan Jr., and B.J. Mokross, Reduced 4f-5d electrostatic interaction of Tm^{2+} in $SrCl_2$, J. Chem. Phys. 5837-5841 (1973) 59.

[12] M. Karbowiak, C. Rudowicz, Trends in Hamiltonian parameters determined by systematic analysis of f-d absorption spectra of divalent lanthanides in alkali-halides hosts: II. $CaCl_2$:Ln^{2+} (Ln = Sm, Eu, Tm, and Yb), J. Lumin. 66-75 (2018) 197.

[13] J. Grimm, O.S. Wenger, K.W. Krämer, H.U. Güdel, 4f-4f and 4f-5d excited states and luminescence properties of Tm^{2+}-doped CaF_2, $CaCl_2$, $SrCl_2$, $BaCl_2$, J. Phys. Chem. B 101-105 (2006) 110.

[14] O.M. ten Kate, K.W. Krämer, E. Van der Kolk, Efficient luminescent solar concentrators based on self-absorption free, Tm^{2+} doped halides, Sol. Energy Mater Sol. Cells 115-120 (2015) 140.

[15] E. Rogers, P. Dorenbos, J.T.M. de Haas, E. van der Kolk, Experimental study of the $4f^n \rightarrow 4f^n$ and $4f^n \rightarrow 4f^{n-1}5d^1$ transitions of the lanthanide diiodides LnI_2 (Ln = Nd, Sm, Eu, Dy, Tm, Yb), J. Phys.: Condens. Matter (2012) 24.

[16] G.H. Dieke, H.M. Crosswhite, The Spectra of the Doubly and Triply Ionized Rare Earths, Appl. Opt. 675-686 (1963) 2.

[17] J. Rubio O., Doubly-Valent Rare-Earth Ions in Halide Crystals, J. Phys. Chem. Solids 101-174 (1991) 52.

[18] P. Dorenbos, Energy of the first $4f^7 \rightarrow 4f^6 5d$ transition of Eu^{2+} in inorganic compounds, J. Lumin. 239-260 (2003) 104.

[19] P. Dorenbos, Anomalous luminescence of Eu^{2+} and Yb^{2+} in inorganic compounds, J. Phys.: Condens. Matter 2645-2665 (2003) 15.

[20] E. van der Kolk, P. Dorenbos, J.T.M. de Haas, and C.W.E. van Eijk, Thermally stimulated electron delocalization and luminescence quenching of Ce impurities in $GdAlO_3$, Phys. Rev. B (2005) 71.

[21] E. van der Kolk, O.M. ten Kate, J.W. Wiegman, D. Biner, K.W. Krämer, Enhanced $^1G_4$ emission in $NaLaF_4$: Pr^{3+}, Yb^{3+} and charge transfer in $NaLaF_4$: $Ce3^+$, Yb3+ studied by fourier transform luminescence spectroscopy, Opt. Mater. 1024-1027 (2011) 33.

[22] M. Hendriks, E. van der Kolk, 4f→5d and anomalous emission in Yb^{2+} doped NaI, SrI_2 and LaI_3 powders prepared by rapid melting and quenching in vacuum, J. Lumin. 231-235 (2018) 207.